THE JOURNAL OF CHEMICAL PHYSICS **133**, 154704 (2010)

Atomic imaging of the monolayer nucleation and unpinning of a compound semiconductor surface during atomic layer deposition

Jonathon B. Clemens,[1] Evgueni A. Chagarov,[1] Martin Holland,[2] Ravi Droopad,[3] Jian Shen,[1,a)] and Andrew C. Kummel[1,b)]
[1]*Department of Chemistry and Biochemistry, University of California, San Diego, 9500 Gilman Dr., La Jolla, California 92093-0358, USA*
[2]*Department of Electronics and Electrical Engineering, University of Glasgow, Glasgow G12 8LT, Scotland*
[3]*Department of Physics, Texas State University-San Marcos, San Marcos, Texas 78666, USA*

(Received 23 April 2010; accepted 17 August 2010; published online 19 October 2010)

The reaction of trimethyl aluminum on the group III rich reconstructions of InAs(0 0 1) and $In_{0.53}Ga_{0.47}As$(0 0 1) is observed with scanning tunneling microscopy/spectroscopy. At high coverage, a self-terminated ordered overlayer is observed that provides the monolayer nucleation density required for subnanometer thick transistor gate oxide scaling and removes the surface Fermi level pinning that is present on the clean InGaAs surface. Density functional theory simulations confirm that an adsorbate-induced reconstruction is the basis of the monolayer nucleation density and passivation. © *2010 American Institute of Physics*. [doi:10.1063/1.3487737]

Atomic layer deposition (ALD) has received attention due to its precise control of film growth at the angstrom scale. ALD has the advantages of uniform growth on three dimensional surfaces because the reactions are self-limiting and it has control over the layer thickness to a fraction of a monolayer (ML).[1–3] These advantages contribute to the wide use of ALD in many applications, especially in gate oxides for microelectronics.[4,5] In metal-oxide-semiconductor field effect transistor (MOSFET) technology, ALD enables the reduction of the equivalent oxide thickness of the gate dielectric to the nanometer scale.[6–8] Additionally, III-V materials are being investigated for use in MOSFETs due to their high electron low field mobility compared to silicon and their tunable band gaps.[4,6,9–12] ALD is the primary technique to form gate oxides on InGaAs(0 0 1).[7,8,12,13]

The choice of ALD precursor for the initial functionalization of the semiconductor surface affects the quality of the III-V/oxide interface.[3,14–16] An ideal interface should consist of ordered, nearly covalent uniform bonding between the dissociation products of the ALD precursor and the semiconductor, leaving the substrate atoms with bulklike bonding; a similar requirement exists for other oxide deposition methods.[17] This requires that the dissociative chemisorption of the ALD precursor does not displace any surface atoms, has a nucleation density of unity, and leaves the surface Fermi level (E_F) unpinned. C-V experiments on MOS capacitors have shown that an unpinned interface can be formed between chemically treated n-$In_{0.53}Ga_{0.47}As$ and ALD grown Al_2O_3 (Ref. 18) with low density of states.[13] This study reports on the first atomically resolved imaging of the metal-first ALD initiation reaction using trimethyl aluminum (TMA) on the group III rich (4×2) surfaces of $In_{0.53}Ga_{0.47}As$(0 0 1) and InAs(0 0 1).

The group III rich (4×2) reconstructions of both InGaAs(0 0 1) and InAs(0 0 1) closely resemble one another.[19–22] Although the larger band gap of InGaAs(0 0 1) makes it preferable for scanning tunneling spectroscopy (STS) experiments and for use in MOSFETs, the InAs(0 0 1)-(4×2) surface exhibits more long range order and fewer defects than InGaAs(0 0 1)-(4×2), so it is preferable for scanning tunneling microscopy (STM) studies of the local bonding environment. The (0 0 1)-(4×2) surfaces lack As dimers, which are key features of the lower temperature (2×4) reconstructions and are known to facilitate the dissociative chemisorption of O_2 and concomitant pinning of the E_F on other III-V surfaces.[23,24] Conversely, the InAs(0 0 1)-(4×2) surface has been shown to have very low reactivity to O_2.[25] This is ideal for ALD because it prevents pinning by adventitious adsorption of O_2. Therefore, InAs(0 0 1)-(4×2) and InGaAs(0 0 1)-(4×2) are hypothesized to be the surfaces most suitable for ALD growth.

The experiments were performed in an ultrahigh vacuum (UHV) chamber equipped with an Omicron low-temperature STM and an Omicron monochromatic x-ray photoelectron spectrometer (XM 1000 MkII with SPHERA analyzer) at a base pressure of 2×10^{-11} Torr. The InAs and $In_{0.53}Ga_{0.47}As$ samples were grown using molecular beam epitaxy offsite on commercially available InAs and InP substrates, as described elsewhere.[22,25] The As_2 capping layer is used for protection against surface oxidation. The InAs samples were degassed at 200 °C for 3 h and heated to 380 °C for 2 h to desorb the As_2 cap. The desired InAs(0 0 1)-(4×2) reconstruction was obtained by increasing the substrate temperature by 0.2 $°C\ s^{-1}$ to 450 °C and holding for 10 min. Surface periodicity was confirmed using low energy electron diffraction (LEED) and STM.[25] The InGaAs(0 0 1)-(4×2) surfaces was prepared similarly as the InAs(0 0 1)-(4×2) surface.[26] Surface periodicity was confirmed using LEED and STM. The III-V semiconductors were transferred into a high vacuum chamber ($P\cong5\times10^{-7}$ Torr) for dosing with TMA.

[a)] Electronic mail: jimshen@ucsd.edu.

[b)] Author to whom correspondence should be addressed. Electronic mail: akummel@ucsd.edu. Tel.: (858) 534-3368. FAX: (858) 534-2063.

The TMA (vapor deposition grade, Sigma-Aldrich) was in a 1% mixture with N_2 carrier gas (99.99% purity). Assuming none of the TMA reacts with the walls of the dosing chamber, the TMA doses ranged from 6000 to 1,800,000 L; however, the lack of wall reactions could not be verified. After 25 °C dosing at pressures from 0.6 to 4 Torr, the samples were reintroduced into the UHV chamber and subsequently annealed to 200 or 300 °C for 1 min. The higher annealing temperature was used for the lowest doses since it provided better STM images, but there was no substantial difference in the observed adsorption sites. The annealing temperatures are approximate since in the Omicron low-temperature STM the thermocouple is not directly on the sample plate. Filled state STM images were acquired from −2.00 to −3.00 V sample bias relative to the electrochemically etched W tip. The constant-current images were taken at a tunneling current set point of 50–100 pA. STS was performed via the fixed tip-sample method using a lock-in amplifier (with a sine wave reference signal of 50 mV and 1.5 kHz) to obtain the dI/dV data from the I(V) output of the Omicron MATRIX electronics. Averaged spectra are reported.

All density functional theory (DFT) simulations were performed with the Vienna *ab initio* simulation package (VASP)[27,28] using projector augmented-wave (PAW) pseudopotentials (PPs)[29,30] and the Perdew–Burke–Ernzerhof (PBE) exchange-correlation functional.[31,32] The choice of PBE functional and PAW PP was validated by parametrization runs demonstrating good reproducibility of experimental lattice constants, bulk moduli, and formation energies for bulk crystalline GaAs and InAs. A Brillouin zone integration was performed at $4\times4\times1$ Monkhorst–Pack k-point mesh with eight irreducible k-points and a plane wave energy cutoff of 400 eV. A double (0 0 1)-(4×2) reconstructed unit cell (∼16.95 Å×16.95 Å, 212 atoms) was used, consisting of eight atomic layers. The bottom layer As atoms were passivated by H atoms with fractional $3/4\ e^-$ charge to mimic a continuous InGaAs bulk according to Ref. 33. The slabs were relaxed using conjugate-gradient relaxation algorithms with 0.05 eV/Å force tolerance level. During relaxation, the three bottom layers were fixed in their bulk positions. The vacuum layer of ∼12 Å was added over the slabs to eliminate spurious interaction through periodic boundary conditions. To compensate for spurious electric fields induced by periodic boundary conditions for this type of system, a dipole correction was applied.[27,28,34] The preliminary $In_{0.5}Ga_{0.5}As$ bulk unit cell was formed from the GaAs unit cell by substituting half of Ga atoms by In atoms following checkerboard pattern and DFT optimizing the lattice constant of the alloy to equilibrium value.

The InAs(0 0 1)-(4×2) surface has been imaged using STM, and the results are discussed elsewhere.[19,25] The clean $\beta3'(4\times2)$ surface reconstruction consists of rows of In atoms along the [1 1 0] direction divided by trough regions that contain two In–In dimers per unit cell in the third atomic layer [see Fig. 1(a)]. For low exposure to TMA followed by UHV annealing, doublet adsorption sites are observed in the trough region of the surface, as shown in Fig. 1(b) by the white arrow. There are a variety of dimer/monomer ratio reports.[35–39] However, to the best of our knowledge, there is no direct experimental measurement. Most probably, at 300 K, TMA exists in the gas phase as a mixture of monomers and dimers with the monomers in excess at low pressure. It is expected that the first step in surface reaction would be physisorption, followed by the chemisorption of aluminum alkyl adsorbates. In this case, observation of pair of sites is consistent with either selective adorption of the dimers or stabilization of the precursors in paired sites on the opposite edges of the neighboring rows to bridge across the trough regions. TMA undergoes dissociative chemisorption to form a dimethyl aluminum (DMA) species bound to the surface, as seen in ALD experiments.[5] The CH_3 product was not observed by STM after the 200 °C annealing, consistent with the weak binding of CH_3 to III-V surfaces.[40,41] Furthermore, the x-ray photoelectron spectroscopy (XPS) measured ratio (see below) of Al to C of 0.5 is consistent with the dissociated methyl group desorbing from the surface below 200 °C. It is noted that the STM height of DMA is at the same STM

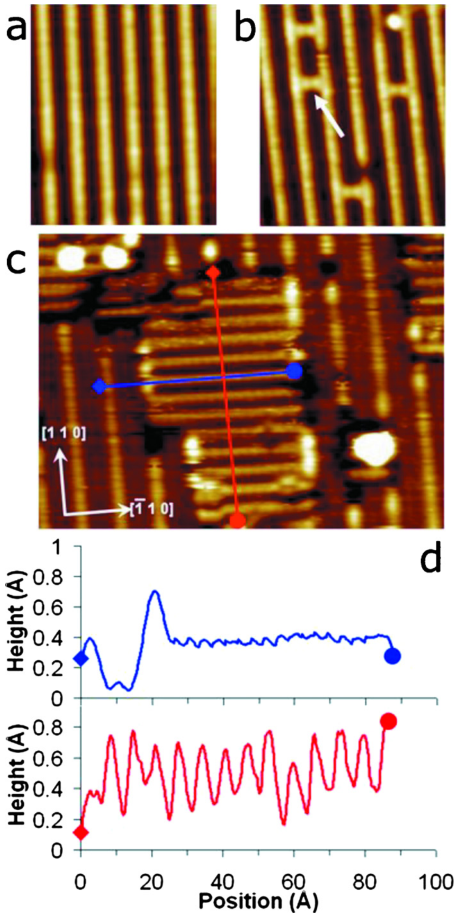

FIG. 1. (a) STM image (−2.00 V, 100 pA) of a 130 Å×110 Å region of the clean InAs(0 0 1)-(4×2) surface. (b) STM image (−2.00 V, 100 pA) of a 130 Å×110 Å region of the InAs(0 0 1)-(4×2) surface after a low exposure to TMA with 300 °C postdeposition annealing (PDA), showing the adjacent reaction sites that bridge the rows; the white arrows show doublet adsorption sites observed in the trough region of the surface. (c) STM image (−3.00 V, 100 pA) of a 135 Å×180 Å region of the surface after a higher TMA dose with 200 °C PDA, showing the formation of ordered domains of TMA-induced reaction that forms rows in the [$\bar{1}$ 1 0] direction. (d) The line trace data for the corresponding line traces in (c). The blue line shows periodicity along the rows of 4.3±0.8 Å and the red line shows periodicity between the rows of 7.9±0.9 Å.

height as the InAs rows within limits of resolution. A control experiment was performed, whereby the sample was exposed at 25 °C in the ALD chamber only to the N_2 carrier gas only followed by the identical annealing regime in the UHV chamber. The STM imaged showed surface disorder and no evidence of the ordered structure observed after exposure to both N_2 carrier gas and TMA. This is consistent with chemisorption of background H_2O in the dosing chamber in the absence of TMA.[42]

When the substrate is dosed with a higher amount of TMA and subsequently annealed at 200 °C, the surface shows a more ordered reconstruction. A typical intermediate coverage (0.25 ML) is shown in Fig. 1(c). The ordered reconstruction forms rows of bright lobes spaced evenly at 4.3 ± 0.8 Å and oriented in the $[\bar{1}\ 1\ 0]$ direction (horizontal). The row-to-row distance in the $[1\ 1\ 0]$ direction (vertical) is 7.9 ± 0.9 Å. Note that the detailed DFT model for adsorption sites explained below leads to new features running in the $[\bar{1}\ 1\ 0]$ direction (horizontal) across the original clean surface features (vertical). The image in Fig. 1(c) also show rows running in the $[1\ 1\ 0]$ direction (vertical) on the left and right sides of the image. Those regions are unchanged from the original surface with a spacing of ~17 Å. The line traces from Fig. 1(c) are shown in Fig. 1(d). Since the height of DMA is approximately the same as the height of the row atoms [Fig. 1(b)], the bright sites could be a mix of row atoms and DMA chemisorbates.

The full coverage structure of DMA/InAs is shown in Fig. 2(a). The highly ordered islands of TMA-induced regrowth seen for the 0.25 ML coverage do not coalesce into large conformal overlayers even at full coverage. The domain sizes vary greatly, from ~50 to ~4000 $Å^2$. At domain boundaries, there is frequently an ~4 Å shift in the $[1\ 1\ 0]$ direction between neighboring regrowth rows (a shift of ~4 Å is consistent with $\frac{1}{2}$ unit cell length of the underlying substrate). A STM image of full coverage DMA/InGaAs(0 0 1)-(4×2) is shown in Fig. 2(b). The domain sizes for full coverage on InGaAs are similar, ranging from single sites to ~3000 $Å^2$. Additionally, using the Al_{2s} peak for XPS analysis, the Al to C ratio is ~0.5 at very glancing take-off angles, which supports that the adsorbed species is DMA. Chemical shift measurements are best performed with the Al_{2p} peak, which has lower intensity than the Al_{2s} peak and, therefore, requires a larger sample for glancing take-off angle XPS.[43,44]

Averaged STS dI/dV measurements of the as-prepared InGaAs(0 0 1)-(4×2) surface and also of the full coverage (1 ML) DMA-passivated InGaAs(0 0 1)-(4×2) surface are shown in Fig. 3. In Fig. 3(a) the clean p-type InGaAs sample (represented by the red solid line) shows the Fermi level, E_F (0 V), near the valence band maximum (0.2 eV above the VBM). After TMA passivation, the STS shows that E_F has not changed with respect to the VBM (the blue dashed line). The density of states has increased near the conduction band onset, but the position of the conduction band minimum (CBM) relative to E_F is similar to the clean surface (0.5–0.6 eV above E_F).

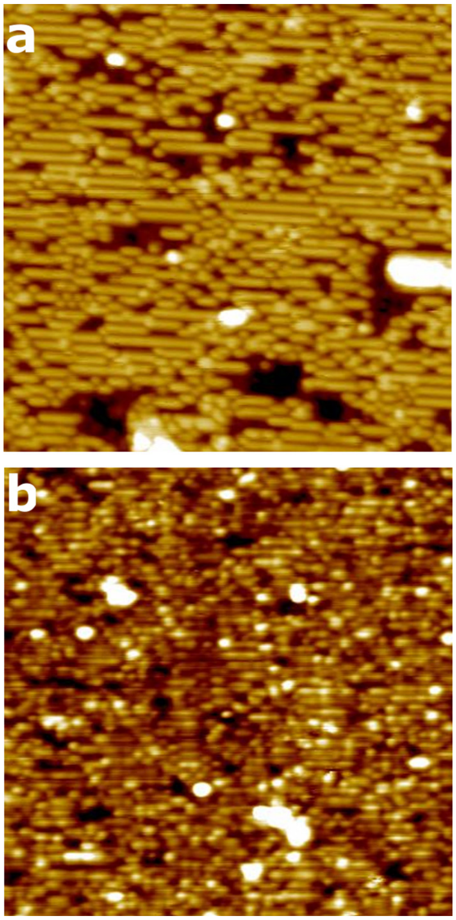

FIG. 2. (a) 345 Å×345 Å STM image of the full coverage TMA-induced reaction on the InAs(0 0 1)-(4×2) surface, showing small domains consisting of horizontal rows in the $[\bar{1}\ 1\ 0]$ direction. (b) 345 Å×345 Å STM image of the same reaction occurring on the InGaAs(0 0 1)-(4×2) surface, which also results in domains consisting of horizontal rows in the $[\bar{1}\ 1\ 0]$ direction. In both cases, the annealing temperature was 200 °C and the STM set points were −2.50 V and 50 pA.

In Fig. 3(b), the clean n-type InGaAs sample (represented by the red solid line) also shows the E_F near the VBM. This is consistent with the surface Fermi level being pinned for clean InGaAs(0 0 1)-(4×2) and is usually attributed to either a large surface dipole or pinning induced by the trough group III dimers.[22] In order for TMA to effectively passivate the surface for the ALD initiation step, the surface E_F must be unpinned. The blue dashed line in Fig. 3(b) shows the averaged dI/dV after the full coverage (1 ML) passivation by DMA on the n-type InGaAs. The STS results show the E_F shifts to about 0.1 eV below the CBM and about 0.6 eV above the VBM. The density of states also increases near the conduction band onset for the n-type material, similar to the results for the p-type material. The STS results for TMA passivation on both n- and p-type InGaAs(0 0 1)-(4×2) are consistent with having formed an unpinned interface which will effectively act as an ALD initiation step for the growth of Al_2O_3 on InGaAs(0 0 1)-(4×2).

The periodicity observed in STM for the TMA-induced reaction [Fig. 1(c)] requires modification of the $\beta 3'(4\times 2)$ surface reconstruction of In(Ga)As(0 0 1)-(4×2). The $\beta 3'(4\times 2)$ structure is illustrated in Fig. 4(a), and Fig. 4(b)

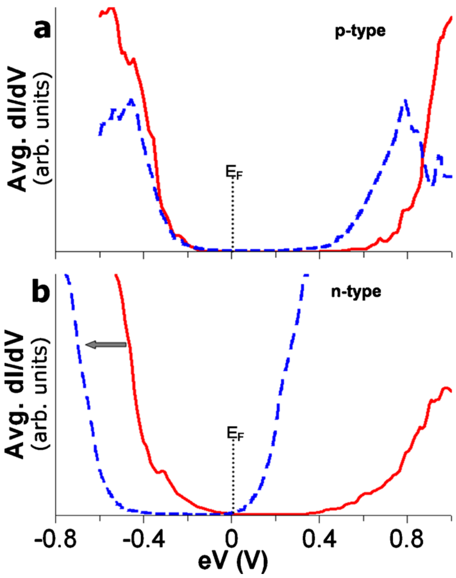

FIG. 3. The average STS dI/dV results from the clean (red solid lines) vs ML TMA reaction (blue dashed lines) of the InGaAs(0 0 1)-(4×2) surface. (a) Both the clean surface and the surface after full ML coverage of TMA-induced surface reaction for the p-type substrates. The E_F position is unchanged with respect to the VBM. (b) The clean n-type surface shows a p-type behavior, consistent with a pinned surface Fermi level. After full ML coverage of TMA-induced surface reaction, the E_F shifts toward the CBM and away from the VBM. The results from both n- and p-type InGaAs(0 0 1) substrates are consistent with passivation of the surface via TMA reaction.

shows the proposed adsorbate-induced reconstruction to obtain the correct periodicity for adsorption sites. This proposed $\iota(2\times 2)$ reconstruction provides chemisorption sites with the observed periodicity and also the dark regions observed between the new adsorbate rows oriented in the $[\bar{1}\ 1\ 0]$ direction; no atoms are lost or gained in forming this structure. In the absence of adsorbates, the new $\iota(2\times 2)$ reconstruction [Fig. 4(b)] is less stable than the $\beta 3'(4\times 2)$ reconstruction by 0.92 eV per double unit cell as calculated by DFT. However, the reaction is driven by the stability gained when DMA forms the new chemisorption sites [Fig. 4(c)]. The desorption energy of a DMA molecule from the As bridge-bonding site in Fig. 4(c) is 2.85 eV with respect to the $\iota(2\times 2)$ surface. Conversely, for the clean surface $\beta 3'(4\times 2)$ reconstruction, DMA can only form single bonds to tricoordinated As atoms, with a desorption energy of 2.64 eV. These tricoordinated As atoms are on the second atomic layer at the edge of the group III row atoms. Bonding to these As atoms causes the DMA molecule to protrude out over the trough region. Additionally, the desorption energy per DMA from the row group III atoms of the $\beta 3'(4\times 2)$ reconstruction is only 1.25 eV but is 2.15 eV for the $\iota(2\times 2)$ surface. This stronger bonding of DMA to the $\iota(2\times 2)$ surface compared to the $\beta 3'(4\times 2)$ surface drives the reconstruction. DFT was employed to compare the chemisorption energies using common reference states: $TMA_{(g)}$, $ethane_{(g)}$, and $\beta 3'(4\times 2)$ surface,

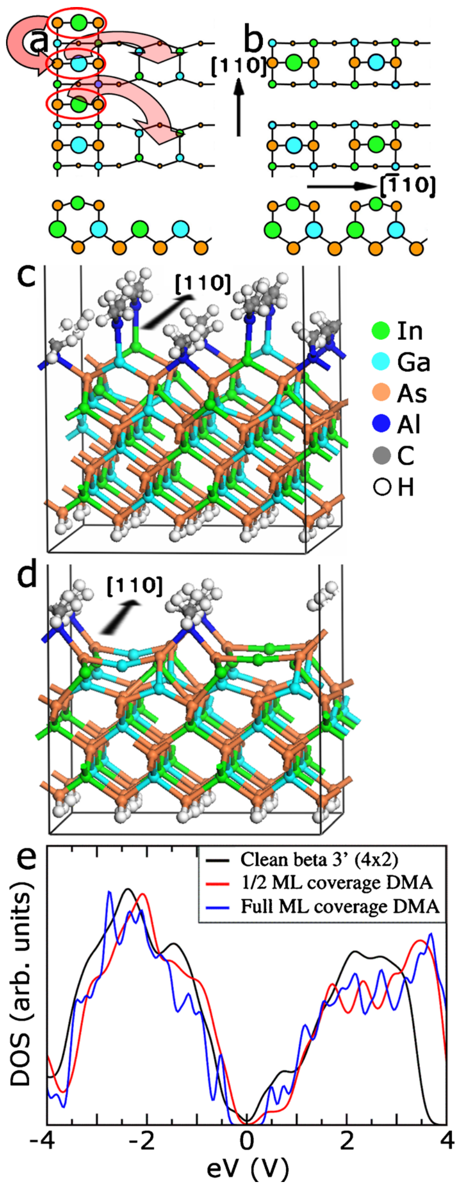

FIG. 4. (a) Top (upper) and side (lower) views of the $\beta 3'(4\times 2)$ reconstruction of the $In_{0.53}Ga_{0.47}As$(0 0 1) surface. The red arrows indicate the necessary movement of surface atoms to form the $\iota(2\times 2)$ reconstruction. (b) Top (upper) and side (lower) views of the $\iota(2\times 2)$ reconstruction of $In_{0.53}Ga_{0.47}As$(0 0 1) that gives the necessary bonding sites corresponding to the observed periodicity change in STM. (c) The DFT ball-and-stick diagram of the full ML DMA adsorption. (d) The DFT ball-and-stick diagram of the $\frac{1}{2}$ ML DMA adsorption. (e) DOS for the DFT slabs shown compared to the clean InGaAs(0 0 1) surface (black line). Note that the clean surface has midgap state density, while the DMA full (blue line) and $\frac{1}{2}$ (red line) ML coverage structures have no state density at E_F.

$$4(CH_3)_3Al_{(g)} + \beta 3'(4\times 2)_{(s)} \rightarrow 4(CH_3)_2Al{:}\beta 3'(4\times 2)_{(s)} + 2CH_3CH_{3(g)}, \quad -0.89\ \text{eV}, \tag{1}$$

$$8(CH_3)_3Al_{(g)} + \beta 3'(4\times 2)_{(s)} \rightarrow 8(CH_3)_2Al{:}\beta 3'(4\times 2)_{(s)} + 4CH_3CH_{3(g)}, \quad -0.54\ \text{eV}, \tag{2}$$

$$4(CH_3)_3Al_{(g)} + \beta 3'(4 \times 2)_{(s)} \rightarrow 4(CH_3)_2Al{:}\iota(2 \times 2)_{(s)} + 2CH_3CH_{3(g)}, \quad -0.87\ \text{eV}, \tag{3}$$

$$8(CH_3)_3Al_{(g)} + \beta 3'(4 \times 2)_{(s)} \rightarrow 8(CH_3)_2Al{:}\iota(2 \times 2)_{(s)} + 4CH_3CH_{3(g)}, \quad -0.63\ \text{eV}. \tag{4}$$

The structures for the full ML and $\frac{1}{2}$ ML coverages on the new $\iota(2\times2)$ reconstruction are shown in Figs. 4(c) and 4(d). Full ML coverage involves DMA bonding to the group III atoms as well as to As bridge-bonding sites [Eq. (4)]. For $\frac{1}{2}$ ML coverage (4 DMA per double unit cell), the most stable sites on both surfaces have DMA bonding to As atoms [Eq. (3)]. The $\frac{1}{2}$ ML coverage is the most stable since the bridge bonds to As atoms are stronger than the single bonds to the group III atoms. The DFT-calculated chemisorption energy for $\frac{1}{2}$ ML coverage on the $\iota(2\times2)$ surface is nearly identical to that on the $\beta3'(4\times2)$, consistent with the STM data. The full ML coverage is more stable on the $\iota(2\times2)$ reconstruction compared to $\beta3'(4\times2)$ by ~100 meV/TMA. While the full ML structure cannot be completely excluded for high TMA doses, the $\frac{1}{2}$ ML structure seems most consistent with islands structure being identical at medium and high coverages.

STM simulations are not reported because the simple STM simulation program cannot reproduce the clean surface structures due to the difficulty with STM simulations involving surface dicoordinated In atoms and pinned surfaces. Instead, consistency is checked between low and high coverage STM images and interpretations. Isolated, single DMA adsorption sites match the group III row atom height [Fig. 1(b)]. For this reason, using only the DMA As bridge-bonding sites [Fig. 4(d)] and not the DMA group III sites results in a structure that also provides the correct periodicity and row features seen in STM. To further confirm the assigned structure, the electronic density of states (DOS) was calculated with DFT for the structures in Figs. 4(c) and 4(d). The clean unreacted surface has some density of states near E_F, indicative of a pinned surface consistent with experiments. This is the group III rich low-temperature reconstruction from *Shen et al.* (black line, no bandgaps).[22] Conversely, the DFT DOS for $\frac{1}{2}$ and full ML coverage [Fig. 4(e) (red and blue lines, with bandgaps)] shows no density at the E_F. The full ML coverage [Fig. 4(e) (blue line)] has a wide band gap nearly identical to the DFT DOS of unpinned InGaAs(0 0 1), calculated using an identical DFT technique and consistent with elimination of band edge states. The DFT DOS is consistent with the assignment of the $\frac{1}{2}$ ML structure for low coverage and either the $\frac{1}{2}$ or full ML structure for high coverage.

In summary, the results show that the reaction of TMA on the (0 0 1)-(4×2) surfaces of InAs and $In_{0.53}Ga_{0.47}As$ results in flat, ordered surfaces with unity nucleation density that is consistent with the surface E_F being unpinned, as shown via STS. The reaction induces a stable reconstruction in the underlying substrate that does not result in displaced surface adatoms, satisfies the bulklike covalent tetrahedral bonding geometries of the semiconductor's surface group V atoms, and results in flat, self-limited ML growth of dimethyl aluminum. This demonstrates the successful ALD initiation step for the growth of Al_2O_3 on InGaAs(0 0 1)-(4×2) for III-V MOSFETs.

This work was supported by SRC-NCRC (Grant No. 1437.003), FCRP-MSD (Grant No. 887.011), and NSF-DMR (Grant No. 0706243).

[1] T. Suntola and J. Hyvarinen, Annu. Rev. Mater. Sci. **15**, 177 (1985).

[2] T. Suntola, Mater. Sci. Rep. **4**, 261 (1989).

[3] M. Ritala and M. Leskela, *Handbook of Thin Film Materials* (Academic, San Diego, 2002), Vol. 1, Chap. 2.

[4] Y. N. Sun, E. W. Kiewra, S. J. Koester, N. Ruiz, A. Callegari, K. E. Fogel, D. K. Sadana, J. Fompeyrine, D. J. Webb, J. P. Locquet, M. Sousa, R. Germann, K. T. Shiu, and S. R. Forrest, IEEE Electron Device Lett. **28**, 473 (2007).

[5] R. L. Puurunen, J. Appl. Phys. **97**, 121301 (2005).

[6] Y. Xuan, Y. Q. Wu, H. C. Lin, T. Shen, and P. D. Ye, IEEE Electron Device Lett. **28**, 935 (2007).

[7] N. Goel, P. Majhi, C. O. Chui, W. Tsai, D. Choi, and J. S. Harris, Appl. Phys. Lett. **89**, 163517 (2006).

[8] S. Koveshnikov, N. Goel, P. Majhi, H. Wen, M. B. Santos, S. Oktyabrsky, V. Tokranov, R. Kambhampati, R. Moore, F. Zhu, J. Lee, and W. Tsai, Appl. Phys. Lett. **92**, 222904 (2008).

[9] M. Passlack, R. Droopad, K. Rajagopalan, J. Abrokwah, R. Gregory, and D. Nguyen, IEEE Electron Device Lett. **26**, 713 (2005).

[10] N. Li, E. S. Harmon, J. Hyland, D. B. Salzman, T. P. Ma, Y. Xuan, and P. D. Ye, Appl. Phys. Lett. **92**, 143507 (2008).

[11] I. Ok, H. Kim, M. Zhang, F. Zhu, S. Park, J. Yum, H. Zhao, D. Garcia, P. Majhi, N. Goel, W. Tsai, C. K. Gaspe, M. B. Santos, and J. C. Lee, Appl. Phys. Lett. **92**, 202903 (2008).

[12] Y. Xuan, Y. Q. Wu, and P. D. Ye, IEEE Electron Device Lett. **29**, 294 (2008).

[13] H. C. Chiu, L. T. Tung, Y. H. Chang, Y. J. Lee, C. C. Chang, J. Kwo, and M. Hong, Appl. Phys. Lett. **93**, 202903 (2008).

[14] B. Brennan, M. Milojevic, H. C. Kim, P. K. Hurley, J. Kim, G. Hughes, and R. M. Wallace, Electrochem. Solid-State Lett. **12**, H205 (2009).

[15] S. Baldovino, S. Spiga, G. Scarel, and M. Fanciulli, Appl. Phys. Lett. **91**, 172905 (2007).

[16] A. Delabie, A. Alian, F. Bellenger, M. Caymax, T. Conard, A. Franquet, S. Sioncke, S. Van Elshocht, M. M. Heyns, and M. Meuris, J. Electrochem. Soc. **156**, G163 (2009).

[17] M. J. Hale, J. Z. Sexton, D. L. Winn, A. C. Kummel, M. Erbudak, and M. Passlack, J. Chem. Phys. **120**, 5745 (2004).

[18] B. Shin, J. Cagnon, R. D. Long, P. K. Hurley, S. Stemmer, and P. C. McIntyre, Electrochem. Solid-State Lett. **12**, G40 (2009).

[19] D. L. Feldwinn, J. B. Clemens, J. Shen, S. R. Bishop, T. J. Grassman, A. C. Kummel, R. Droopad, and M. Passlack, Surf. Sci. **603**, 3321 (2009).

[20] U. Seidel, B. E. Sagol, C. Pettenkofer, and T. Hannappel, Appl. Surf. Sci. **255**, 722 (2008).

[21] C. Kendrick, G. LeLay, and A. Kahn, Phys. Rev. B **54**, 17877 (1996).

[22] J. Shen, J. B. Clemens, E. A. Chagarov, D. L. Feldwinn, W. Melitz, T. Song, S. Bishop, A. C. Kummel, and R. Droopad, Surf. Sci. **604**, 1757 (2010).

[23] P. Kruse, J. G. McLean, and A. C. Kummel, J. Chem. Phys. **113**, 9224 (2000).

[24] D. L. Winn, M. J. Hale, T. J. Grassman, J. Z. Sexton, and A. C. Kummel, J. Chem. Phys. **127**, 134705 (2007).

[25] J. B. Clemens, S. R. Bishop, D. L. Feldwinn, R. Droopad, and A. C. Kummel, Surf. Sci. **603**, 2230 (2009).

[26] J. Shen, D. L. Winn, W. Melitz, J. B. Clemens, and A. Kummel, ECS Trans. **16**(5), 463 (2008).

[27] G. Kresse and J. Furthmuller, Comput. Mater. Sci. **6**, 15 (1996).
[28] G. Kresse and J. Furthmuller, Phys. Rev. B **54**, 11169 (1996).
[29] P. E. Blöchl, Phys. Rev. B **50**, 17953 (1994).
[30] G. Kresse and D. Joubert, Phys. Rev. B **59**, 1758 (1999).
[31] J. P. Perdew, K. Burke, and M. Ernzerhof, Phys. Rev. Lett. **77**, 3865 (1996).
[32] J. P. Perdew, K. Burke, and M. Ernzerhof, Phys. Rev. Lett. **78**, 1396 (1997).
[33] K. Shiraishi, J. Phys. Soc. Jpn. **59**, 3455 (1990).
[34] J. Neugebauer and M. Scheffler, Phys. Rev. B **46**, 16067 (1992).
[35] Ch. Henricks and D. P. Eyman, Inorg. Chem. **6**, 1461 (1967).
[36] J. O. Carlsson, S. Gorbatkin, D. Lubben, and J. E. Greene, J. Vac. Sci. Technol. B **9**, 2759 (1991).
[37] T. Beuermann and M. Stuke, Appl. Phys. B: Photophys. Laser Chem. **49**, 145 (1989).
[38] Y. Zhang and M. Stuke, Jpn. J. Appl. Phys., Part 2 **27**, L1349 (1988).
[39] J. L. Brum, P. Tong, and B. Koplitz, Appl. Phys. Lett. **56**, 695 (1990).
[40] D. W. Squire, C. S. Dulcey, and M. C. Lin, Chem. Phys. Lett. **116**, 525 (1985).
[41] J. R. Creighton, Surf. Sci. **234**, 287 (1990).
[42] J. B. Clemens, R. Droopad, and A. C. Kummel, Surf. Sci. **604**, 1859 (2010).
[43] M. Milojevic, F. S. Aguirre-Tostado, C. L. Hinkle, H. C. Kim, E. M. Vogel, J. Kim, and R. M. Wallace, Appl. Phys. Lett. **93**, 202902 (2008).
[44] A. P. Kirk, M. Milojevic, J. Kim, and R. M. Wallace, Appl. Phys. Lett. **96**, 202905 (2010).